Check for updates

Optimization of trimetallic Cu–Cr–Ca nanoparticle-catalyzed transesterification of amla (*Phyllanthus emblica* L.) seed oil: analytical characterization and fuel properties of biodiesel†

Humaira Kanwal,[ab] Farooq Anwar,*[acd] Ahsan Tanvir, [b] Syed Hussain Imam Abidi[e] and Muhammad Waseem Mumtaz[f]

Renewable energy sources are experiencing a surge in demand, motivating substantial study into biodiesel synthesis from non-edible oil sources as a strategy to offset the conflict between food and fuel. The present work focuses on optimizing the trimetallic Cu–Cr–Ca oxide nanoparticle-catalyzed transesterification of a non-food amla (*Phyllanthus emblica* L.) seed oil, producing high yields of good quality amla oil methyl esters (AOMEs)/biodiesel. Response surface methodology was used to optimize the transesterification process by employing a central composite design with a total of 30 experimental trials, including (2^4) factorial, (2(2)) axial, and (6) central points. The transesterification process was catalyzed by a newly synthesized trimetallic Cu–Cr–Ca nano-catalyst. Statistical analysis demonstrated the model's significance ($p < 0.0001$) with a high predicted R^2 value (0.9958) closely aligned with an adjusted R^2 value (0.9982). The optimal AOME yield of 92% was achieved at a 9 : 1 methanol-to-oil molar ratio, using 3 g of Cu–Cr–Ca catalyst at 85 °C and 5 h. GC-MS analysis of the produced methyl esters revealed the presence of 85.98% unsaturated and 14.03% saturated fatty acids, indicating the successful accomplishment of the transesterification reaction. FTIR ester stretching peaks at 1734 and 1739 cm^{-1} further confirmed the completion of transesterification. The fuel properties of AOMEs show potential as an alternative green energy fuel compared with ASTM standards, supporting the optimized nano-catalyzed transesterification for producing *Phyllanthus emblica* L. seed oil biodiesel with acceptable physico-chemical properties.

1 Introduction

Fossil fuels currently provide majority of the world's energy needs, resulting in the emission of pollutants like SO_2, NO_x, CO_2, and other greenhouse gases that are irreversibly altering the climate. Moreover, fossil fuels are not renewable due to their limited availability and expected depletion.[1–3] Hence, developing alternative renewable and green fuels like biofuels is crucial for sustainability and environmental protection.[4,5] Currently, about 80% of the global liquid biofuel production consists of bioethanol, while the remaining 20% is produced as biodiesel.[6] Biodiesel is valued as a sustainable, biodegradable, and eco-friendly biofuel owing to its superior exhaust emission profile and higher cetane number.[2,7]

Transesterification is recognized as the preferred method for biodiesel synthesis due to its operational ease and economic feasibility.[8] In this process, triglycerides and alcohols undergo a sequence of reversible reactions, which first converts them into diglycerides and then into monoglycerides, with glycerine obtained as a secondary product.[9–12] However, the yield, quality characteristics and fuel properties of biodiesel can be further improved by optimizing transesterification variables.[5,13] Transesterification of oils and fats can be done catalytically or non-catalytically. Triglycerides are catalytically transesterified utilizing a range of catalysts like homo/heterogeneous acid–base catalyst, mixed oxides or oxides from natural resources and enzymes.[14,15] Despite the effectiveness of catalysts, homogeneous catalysts cause soap formation and result in low biodiesel yield, and heterogeneous catalysts have lower reaction rates,

aInstitute of Chemistry, University of Sargodha, Sargodha 40100, Pakistan. E-mail: farooq.anwar@uos.edu.pk; fqanwar@yahoo.com

bApplied Chemistry Research Center, Pakistan Council of Scientific and Industrial Research Laboratories Complex, Ferozepur Road, Lahore 54600, Pakistan

cDepartment of Food Science, Faculty of Food Science & Technology, Universiti Putra Malaysia, 43400 Serdang, Selangor, Malaysia

dFaculty of Health Sciences, Shinawatra University, 99 Moo 10, Bangtoey, Samkhok, Pathum Thani 12160, Thailand

ePakistan Council of Scientific and Industrial Research, 01 Constitution Avenue, G-5/2, Islamabad, Pakistan

fDepartment of Chemistry, University of Gujrat Hafiz Hayat Campus, Jalalpur Road, Gujrat, Pakistan

† Electronic supplementary information (ESI) available. See DOI: https://doi.org/10.1039/d5ra00098j

while enzymatic catalysts are selective, expensive and less stable.[16]

The world is experiencing a revolution in research across various fields due to the remarkable advancements in nanomaterials.[17–22] In recent research, nanocatalysts have emerged as a promising alternative in catalytic transesterification.[23] Nanocatalysts are usually pseudo-homogeneous catalysts, offering the advantage of both homo/heterogeneous catalysts in terms of activity, selectivity, efficiency and reusability.[24,25] Nanocatalysts exhibit superior catalytic properties due to their large surface-to-volume ratio and high porosity, enabling increased reactant interaction with active sites which results in an enhanced reaction rate.[26] Nanocatalysts characteristics like acidity or basicity, catalyst active site and porosity are customizable and can be fabricated as per requirements to achieve the maximum efficiency. Munir et al. (2021) optimized methyl ester production from non-edible Celastrus paniculatus Willd. oil using trimetallic (Ce, Cu, and La) based montmorillonite nanocatalyst and obtained a maximum biodiesel yield of 89.42%.[16] In another study, CuO–CaO mixed metal oxide nanoparticles were used as a nanocatalyst for the transesterification of Moringa oleifera seed oil and a high biodiesel yield of 95.24% was achieved. The optimized reaction conditions determined via central composite design included a methanol-to-oil ratio of 0.3 : 1 (vol/vol), 4 wt% catalyst loading, and a reaction duration of 2.5 h.[27] Moreover, the use of nanocatalyst helps to achieve a higher reaction rate, reduced reaction time, improved biodiesel yield, and easy separation, recovery, and reusability by incorporating magnetic nanomaterials.[28]

Response surface methodology (RSM) involving a set of statistical and mathematical techniques can be applied to optimize the process parameters in biodiesel production by fitting a polynomial equation to trial results to accurately describe the dataset behavior and make statistical predictions.[13,29] RSM efficiently reduces the trial counts required to achieve optimum methyl ester yield, resulting in lower production costs.[30] RSM facilitates the examination of interactions among reaction parameters and their impact on the response through 3D graphs.[30,31] Alade et al. (2022) optimized bentonite supported trimetallic Fe–Co–Ni nanocatalyzed biodiesel production from palm kernel oil using Box–Behnken design response surface methodology and obtained an optimal yield of 95.2% yield under the ideal reaction condition of 10 : 1 methanol to oil ratio, 5% (w/w) Fe–Co–Ni, and 55 °C.[32]

Over 350 oil-yielding crops have been discovered globally as possible feedstock of biodiesel production. The potential sources of feedstock fall into four classes: non-edible oils, edible oils, animal fats and waste oils. Notably, the oil source alone constitutes 75% of the overall cost involved in biodiesel production.[9] Among the plethora of potential biodiesel resources, Ullah et al. (2015) identified Phyllanthus emblica L. oil as a feasible non-edible oil source.[33] Amla oil transesterification is investigated using a range of solid base and magnetic oxide catalysts. A 90.31% biodiesel yield is obtained with Fe–Ca magnetic oxide catalyzed transesterification, while a solid base CaO catalyzed process gave a maximum yield of 76.61%. The

lower yield by CaO is primarily because of the drawbacks of heterogeneously catalyzed transesterification. The diffusion limited mass transport in porous materials and pore blocking of the catalyst surface due to deposition of reaction mixture molecules leads to reduced catalytic activity.[34]

Calcium oxide has been studied widely as a heterogeneous catalyst for biodiesel production due to its strong basicity. However, the catalytic activity of CaO is significantly impacted by the presence of moisture, FFA and glycerol. For example, the hydroxides formed as a result of reaction of CaO with moisture deactivate the active sites and promote the leaching of Ca^{2+} into the reaction medium.[35] Additionally, hydroxides generated due to moisture and FFA can result in a saponification reaction forming Ca-soap which deactivates the catalyst sites and hinders biodiesel separation and purification.[36] The glycerol formed during transesterification can also react with CaO, resulting in calcium diglyceroxide formation which further increases leaching and reduces catalyst reusability.[37]

To address these challenges, a Cu–Cr–Ca ternary metal oxide nanocatalyst was chosen due to its novel composition. This catalyst offers a balanced approach, integrating basic (CaO)-, moderate amphoteric (CuO)-, and strong amphoteric (Cr_2O_3) properties, resulting in enhanced bifunctionality. The combination of a basic oxide known for accelerating transesterification with transition metal oxides recognized for their bifunctional nature simultaneously enables transesterification and esterification.[38] This allows simultaneous conversion of triglycerides and free fatty acids in a single step. This synergy enhances the catalyst's tolerance against high free fatty acid (FFA) content and moisture, making it highly effective for biodiesel production from diverse feedstocks. Moreover, the nanoscale size of the Cu–Cr–Ca catalyst significantly improves its catalytic efficiency. The high surface area-to-volume ratio enhances active site availability, promoting better reactant adsorption and facilitating mass transfer, which is often a limiting factor in conventional heterogeneous catalysts.

The effectiveness of mixed metal oxides in improving catalytic activity has been demonstrated in previous studies. For instance, the binary CaO–ZnO catalyst yielded 94% biodiesel in mixed metal oxide-based transesterification of crude jatropha oil (12 wt% FFA), which was higher than that of individual alkaline CaO (91%) and ZnO (41%). The synergistic effect of alkaline CaO and transition metal oxide ZnO, combined with reactive acidic and basic sites for simultaneous esterification and transesterification improves moisture and FFA poisoning resistance and reduces saponification, making it a promising approach for producing methyl ester from low-quality feedstocks.[38]

However, there is a lack of research on RSM based optimization of trimetallic nano-catalyzed transesterification of non-food amla oil for biodiesel synthesis. The current research was planned to optimize the transesterification of amla oil using nanocatalyst to understand the impact of different reaction variables on the percentage yield and quality characteristics of amla oil biodiesel (AOBD). The current research focuses on the use of

newly designed trimetallic (Cu–Cr–Ca) nanocatalyst for the methanolysis of non-edible *Phyllanthus emblica* L. oil to produce AOBD. The trimetallic (Cu–Cr–Ca) nanocatalyst is structurally characterized using SEM, EDX, XRD and FTIR analyses. The transesterification process is optimized *via* RSM to determine the optimal reaction parameters. The qualitative evaluation of the produced AOBD was conducted using GC-MS and FTIR. The fuel properties of AOBD were analyzed and compared with literature values and ASTM standards.

2   Materials and methodology

2.1   Materials

Non-conventional/non-food amla (*Phyllanthus emblica* L.) oil seeds collected from a local market in Lahore, Punjab, Pakistan were used in this study. Initially, the seeds were dehusked and subsequently sun-dried for approximately two weeks. Then, the desiccated seeds were pulverized using an electric crusher to attain a finely powdered form. The resulting powder was carefully packaged in an impermeable plastic container to mitigate the moisture absorption and contamination by other impurities. All additional chemicals and reagents utilized in the study such as carbon tetrachloride (CCl_4), potassium hydroxide (KOH), activated charcoal, chloroform ($CHCl_3$), glacial acetic acid (CH_3COOH), ethanol (C_2H_5OH), methyl orange, methanol (CH_3OH), oxalic acid ($C_2H_2O_4$), potassium iodide (KI), phenolphthalein, ethylene glycol ($C_2H_6O_2$), ethylenediamine ($C_2H_8N_2$), sodium thiosulphate ($Na_2S_2O_3$), starch, isopropanol (C_3H_7OH), sodium acetate (CH_3COONa), sulfuric acid (H_2SO_4), copper chloride ($CuCl_2$), chromium chloride ($CrCl_2$), calcium sulphate ($CaSO_4$), and sodium hydroxide (NaOH) *etc.*, were of high purity and analytical grade from Sigma-Aldrich (USA) and Merck Chemical Company (Darmstadt, Germany).

2.2   Trimetallic Cu–Cr–Ca nanoparticle catalyst synthesis

Cu–Cr–Ca nanocatalyst was synthesized by the co-precipitation method (Fig. 1). Synthesis was carried out by separately dissolving $CaSO_4$ (2.73 g), $CuCl_2$ (2.68 g), and $CrCl_2$ (3.167 g) in 1000 mL of distilled water. Subsequently, equal volumes (500 mL each) of each of the $CaSO_4$, $CuCl_2$, and $CrCl_2$ solutions were mixed in a 5000 mL flask. While stirring the mixture continuously, a 0.02 M NaOH solution was slowly added for precipitation until the 1 : 1 volume ratio was reached. The precipitates were further processed and a fine powder of Cu–Cr–Ca nanocatalyst was obtained. The newly synthesized nanocatalyst was further characterized using SEM, EDX, XRD and FTIR.

2.3   Amla seed oil extraction and physico-chemical analysis

A Soxhlet extractor fed with crushed amla powder along with *n*-hexane as the solvent was utilized for the oil extraction in three successive batches, each run for 6 h. After extraction, *n*-hexane was distilled at 45 °C using a rotary evaporator. Anhydrous sodium sulfate (Na_2SO_4) was added to the recovered oil to eliminate the moisture residue, followed by filtration of the oil. The yield of recovered oil was calculated gravimetrically. AOCS standard methods were employed to analyze the recovered oil for basic physico-chemical properties, including density, iodine value, FFA and saponification value.[39]

2.3.1   Density. Density, defined as mass per unit volume, was determined using a relative density (RD) bottle following the mass-to-volume ratio method with water as the reference standard.

2.3.2   Free fatty acid (FFA) value. FFA in the oil or fats basically exist in distinctive form and are produced as hydrolytic products in the presence of moisture, temperature and oil degradation. It is defined as the amount of KOH (mg) needed to neutralize the free acids present per gram of oil or fat. The FFA of *P. pinnata* oil was predicted by following the standard AOCS technique F 9a-44 (1997).[40] In the FFA assessment of oil, the sample is mixed with HPLC-grade ethyl alcohol and phenolphthalein indicator to form a homogenized mixture. It is then titrated with sodium hydroxide until a stable pink endpoint appears, and the free fatty acid content is calculated as a function of oleic acid using the following formula:
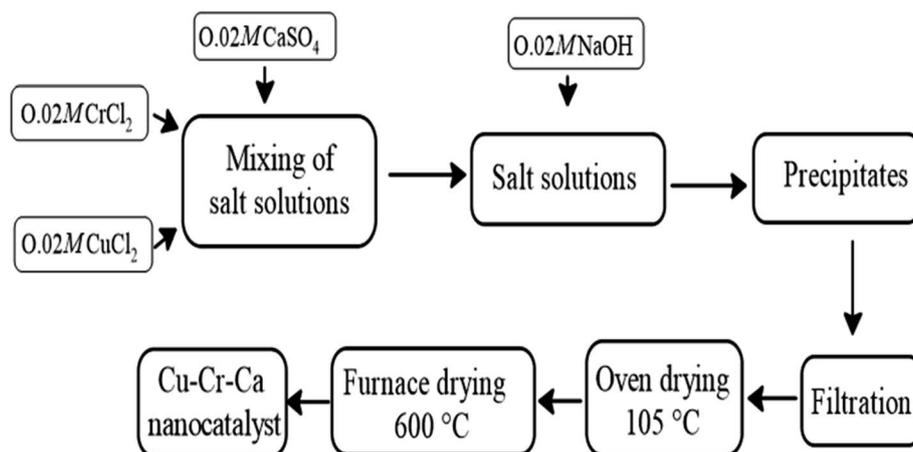

Fig. 1   Flowsheet diagram for the synthesis of trimetallic Cu–Cr–Ca nanocatalyst.

$$\text{FFA\%} = \frac{(\text{vol of NaOH used} \times \text{molecular wt of oleic acid} \times N \text{ of NaOH solution} \times 100)}{(\text{grams of sample analyzed} \times 1000)}$$

2.3.3 Iodine value. The iodine value refers the level of unsaturation of oil or fat. A higher iodine value indicates a high degree of unsaturation. It is stated as "the amount of halogens in grams present in 100 grams of oil or fat and is represented as weight of iodine." Iodine value (IV) determination was made using the standard AOCS technique Cd 1-25 (1997).[40] In iodine value determination, the oil sample was mixed with Wij's solution and CCl_4 under continuous stirring and then kept in the dark for a certain time. The potassium iodide (KI) solution and distilled water was added followed by the addition of starch indicator. The mixture was titrated against the sodium thiosulphate solution until the disappearance of a yellowish iodide colour. The procedure was similarly replicated for the blank solution and the iodine value of the sample oil was determined using the following formula:

$$\text{Iodine value} = \frac{(\text{blank titration value} - \text{sample titration value}) \times N \text{ of Na}_2\text{S}_2\text{O}_3 \text{ used} \times 12.69}{\text{sample oil in grams}}$$

2.3.4 Saponification value. Saponification value estimation was carried out using the standard AOCS technique Cd 3-25 (1997).[40] It is represented as "the number of milligrams (mg) of potassium hydroxide (KOH) necessary for the saponification of 1 g oil or fat." In the saponification value assessment, the oil sample was refluxed with alcoholic KOH and then cooled and titrated with HCl using phenolphthalein as an indicator. A blank solution was processed under identical conditions and the saponification value was determined using the given formula:

$$\text{SV(mg KOH per g)} = \frac{(\text{blank titration value} - \text{sample titration value}) \times N \text{ of HCl used} \times 56.1}{\text{grams of oil}}$$

2.4 Pre-treatment of amla seed oil

For an effective base-catalyzed transesterification, an oil with FFA value below 1% is considered as ideal. However, the extracted amla oil had a higher FFA content of 6.1%. Before proceeding with base catalyzed transesterification, the FFA value of oil needs to be reduced to <1%. To address this issue, an acid-catalyzed esterification process was employed using acidified methanol.[41,42] Esterification utilizing H_2SO_4 as a catalyst was employed to effectively reduce the FFA content by reacting with acidified methanol forming esters. The reaction was carried out at 65 °C for 1 h with 0.5% acid catalyst (w/w oil basis) and continued until the FFA content dropped below 1%. After the pretreatment, the residual CH_3OH was removed from the oil before proceeding with base-catalyzed transesterification.

2.5 Design of experiment *via* response surface methodology

Response surface methodology was utilized to evaluate the optimal conditions of the selected dependent variable using Design-Expert® software version 13 (Stat-Ease, Inc., Minneapolis, MN, USA) for experimental design. A five-level, four-factor central composite design (CCD) with 30 trials ($2^k + 2k + 6$) including 16 factorial and 8 axial runs, with 6 replications at the center point to assess pure error was employed to optimize reaction factors. Biodiesel yield served as the response variable and Table 1 details the response parameters and their ranges.[30,43] A complete design matrix was generated using CCD, and trials were conducted within the specified parameter ranges to measure the percentage response, the biodiesel yield.

2.6 Amla oil biodiesel production

The transesterification reaction was carried out in a 2000 mL (2 L) reactor, which consisted of a three-necked round-bottom flask fitted with a condenser on the side necks, a central mechanical stirrer and a thermometer on the other side neck. Prior to initiating the reaction, 250 g of esterified amla seed oil was heated to a desired temperature. Trimetallic Cu–Cr–Ca nano-catalyst was dissolved in an appropriate amount of CH_3OH, introduced to the preheated amla oil and agitated at a constant rate of 750 rpm for the designated time period.

After completion of the reaction, the reaction mixture was transferred into a separating funnel for phase separation at room temperature. The top layer containing esters (the desired product) was isolated from the glycerol and other residual

Table 1 Variables and their limits for central composite experimental design

| Variable | Symbol | Unit | Range and level | | |
			−1	0	+1
Methanol to amla oil ratio	A	—	6:1	9:1	12:1
Cu–Cr–Ca concentration	B	wt%	2	3	4.0
Temperature	C	°C	80	85	90
Reaction time	D	min	4	5	6

materials in the lower layer. The purified AOMEs layer underwent methanol distillation to eliminate any remaining traces of the solvent. Afterward, the esters underwent successive rinsing with distilled water to eliminate any glycerol or residual catalyst. The esters were then dried using anhydrous sodium sulfate (Na_2SO_4), which serves as a desiccant absorbing any leftover water molecules. After drying, the mixture was filtered to remove any traces of sodium sulfate and residual water from the esters.[39,40]

2.7 Statistical assessment

The examination of data involved the use of Design Expert 13 software to conduct regression analysis and graphical representation. A second order polynomial equation (eqn (1)) serving as the empirical regression model was obtained upon regression analysis of experimental data from the transesterification process. Regression coefficients for the second-order multiple regression models were calculated utilizing data from the CCD for reaction condition optimization.

$$Y = \beta_{k0} + \sum_{i=1}^{k} \beta_{ki} x_i + \sum_{i=1}^{k} \beta_{kii} x_i^2 + \sum_{i=1}^{k} \sum_{j=i+1}^{k} \beta_{kij} x_i x_j + e \quad (1)$$

Eqn (1) represents the expected biodiesel yield (Y). Coefficients β_0, β_i, β_{ii}, and β_{ij} signify intercept, linear, quadratic, and interaction terms. This equation incorporates linear and quadratic effects, as well as variable interactions to optimize fitting to experimental results, with 'e' denoting random error and 'k' indicating the set of parameters investigated and optimized in the trial.[44] The data was subjected to analysis of variance (ANOVA) and the response surfaces were generated to analyze variable interactions. The fit quality of the polynomial model was assessed using R^2 and R_{adj}^2, and statistical significance was confirmed with the F-test and t-test.[43]

2.8 Characterization of AOMEs

Amla oil and AOMEs were analyzed by Fourier transfer infrared (FTIR) spectroscopy for identification of the functional group. The FTIR spectra were recorded of amla oil and biodiesel in the scanning range of 400–4000 cm^{-1} using a Bruker-7600 FTIR spectrometer (Germany). The FTIR spectrum of amla oil was compared with the spectrum of amla biodiesel to identify the changes in functional groups during the transesterification process and to confirm the formation of fatty acid methyl esters (FAMEs). The GC-MS scan was performed to obtain the comprehensive fatty acid profile of the synthesized biodiesel and to identify specific methyl esters formed during the transesterification process.[33] GC-MS analysis on an Agilent system with a DB-5 column (0.25 mm diameter) was performed using a splitless 0.2 μL injection, with column temperature ramped from 70 °C to 260 °C at 4 °C min^{-1}. Helium was used as a carrier gas/mobile phase with flow rate of 1.5 mL min^{-1} and the mass scanning range was adjusted between 50 and 550 m/z. The GC-MS machine's NIST MS library was used to identify the FAMEs, and the composition was expressed as a relative percentage of the total peak area.

2.9 Fuel properties of AOMEs/amla oil biodiesel

Biodiesel fuel properties were determined in triplicate following standard procedures. The cloud point of the *P. emblica* methyl esters was determined using the ASTM D2500 method. ASTM D93 standard was utilized to determine the flash point of biodiesel. The pour point of the AOMEs was assessed using the ASTM D97 standard. Following the ASTM D445 procedure, the kinematic viscosity of the AOMEs was measured at 15 °C with a viscometer. The density of the biodiesel was examined using an analyzer, adhering to the ASTM D1298 protocol. Additionally, the cold filter plugging point (CFPP) of the biodiesel was determined following the ASTM D6371 method.[33,40]

3 Results and discussion

3.1 Physico-chemical properties of crude amla oil

In this investigation, the physico-chemical characterization of amla oil was conducted prior to initiating the base-catalyzed transesterification reaction. *Phyllanthus emblica* L. seed oil had a percentage oil yield of 44% which is less than the 52% reported by Sunil *et al.* (2022).[45] Amla oil had a free fatty acid (FFA) value of 6.1 mg KOH per g, necessitating an initial esterification step to reduce the FFA content to below 1%. The chemical parameters of amla oil were determined as follows: iodine value of 67 g I_2 per 100 g and saponification value of 157 mg KOH per g (Table 2).

3.2 Trimetallic Cu–Cr–Ca nanocatalyst characterization

Trimetallic Cu–Cr–Ca nanoparticle synthesis was confirmed by X-ray diffractometry (XRD). The diffraction peaks were recorded between 20° and 80° with scanning rate of 4° min^{-1} using Cu-Kα = 1.5 Å. In the Cu–Cr–Ca trimetallic nanoparticles (TMNPs), each metal forms its own distinct oxide phase, resulting in separate phases of CuO, Cr_2O_3, and CaO. The XRD spectra of synthesized Cu–Cr–Ca nanoparticles show no significant impurity (Fig. 2). Each peak in the spectra indicates a specific metallic oxide nanoparticle produced. The reported 2θ at 29.38°, 31.39°, 43.15° and 64.65° are indexed to (011), (111), (012) and (113) hkl planes respectively, which correspond to CaO NPs and are consistent with the earlier investigations on CaO NPs reported by Jadhav *et al.* (2022).[46] The diffraction peaks at 24.58°, 33.46°, 35.68°, 39.26°, and 64.65° correlates with the Cr_2O_3 diffraction pattern and are indexed to the (012), (104), (110), (006), and (214) crystallographic planes, respectively. The

Table 2 Physicochemical parameters of *Phyllanthus emblica* L. seed oil

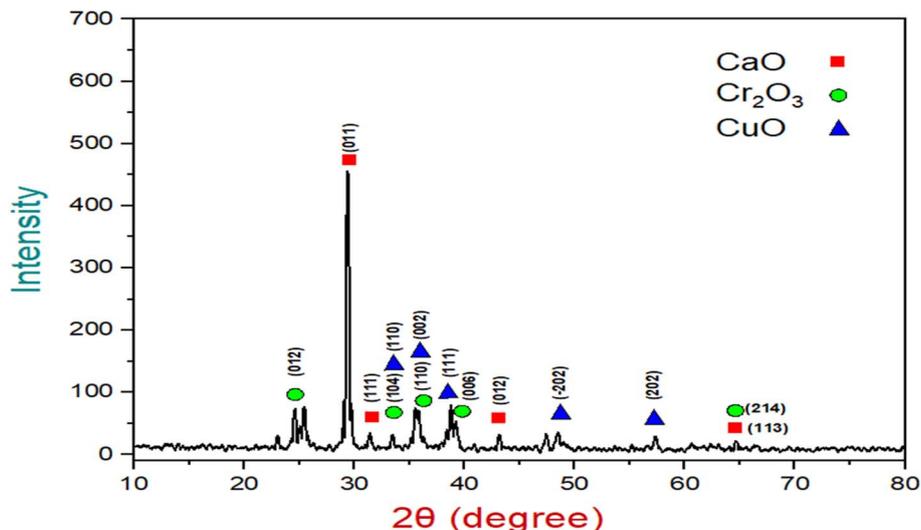| Sr. no.	Parameters	Results
1	Colour	Dark green
2	Odour	Pleasant
3	Yield of oil (%)	44 ± 0.70
4	Density (g mL^{-1}, at 40 °C)	0.95 ± 0.07
5	Free fatty acid value (mg KOH per g)	6.1 ± 0.4
6	Iodine value (g per 100 g)	67 ± 8
7	Saponification number (mg KOH per g)	157 ± 12

Fig. 2 XRD pattern of the trimetallic Cu–Cr–Ca nanocatalyst.

peaks obtained for Cr_2O_3 NPs are well aligned with the previously reported Cr_2O_3 NPs by David *et al.* (2023).[47] Meanwhile, the 2θ peaks at 33.46°, 35.68°, 38.75°, 48.46°, and 57.33° belong to CuO nanoparticles and are attributed to Miller–Bravais indices of (110), (002), (111), (−202), and (202), respectively and align well with the earlier work by Mobarak *et al.* (2022) on CuO NPs.[48] The crystal size of prepared Cu–Cr–Ca NPs are between 12 and 38 nm determined using the Scherrer equation, as presented in (S1).† The average crystallite size of 25.79 nm confirms the Cu–Cr–Ca material as a nanocatalyst. In a study by Vaseghi *et al.* (2018), the XRD pattern of Cu–Cr–Ni nanoparticles showed diffraction peaks at 34°, 36°, 38°, and 44°, which are comparable with the Cu–Cr–Ca trimetallic NPs.[49]

Scanning electron microscopic (SEM) analysis further validates the crystalline structure of synthesized Cu–Cr–Ca nanocatalyst observed in XRD analysis with abundant pores (Fig. 3). The large number of pores are responsible for the abundant active sites on the catalyst surface, which results in an enhanced reaction rate because of more contact of reactants to active sites. The present study elucidates the morphological features of

synthesized Cu–Cr–Ca nanocatalyst with uniform composition and degree of agglomeration. Yasmeen *et al.* (2023) suggests that the weak forces are responsible for the adhesion of nanoparticles to each other, resulting in agglomeration between fine nanoparticles.[50]

EDX analysis between the energy range of 0 to 10 keV was employed to study the quantitative and qualitative aspects of synthesized trimetallic nanocatalyst. The EDX spectra in Fig. 4 reports the oxides of Cu–Cr–Ca nanoparticles. Exposure of the subject sample to energy between a given range results in the emission of characteristic X-rays, each of which specifically belong to certain elements. The specific elemental characteristic X-rays obtained in the present EDX analysis shows the elemental peaks of Cu–Cr–Ca and oxygen due to the oxide nature of formed nanoparticles with composition ratios of Ca (18.08%), Cu (23.39%), Cr (17.63%) and O (40.90%). The ratio of Cu–Cr–Ca TMNPs calculated based on their percentage is 1.33 : 1 : 1.02.

The FTIR spectrum in the scanning rage of 650–4000 cm^{-1} shows the functional group analysis of the synthesized Cu–Cr–
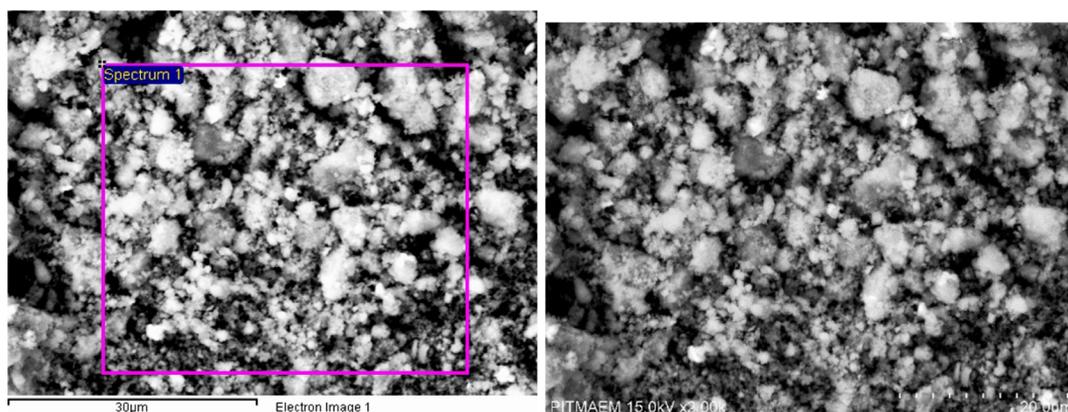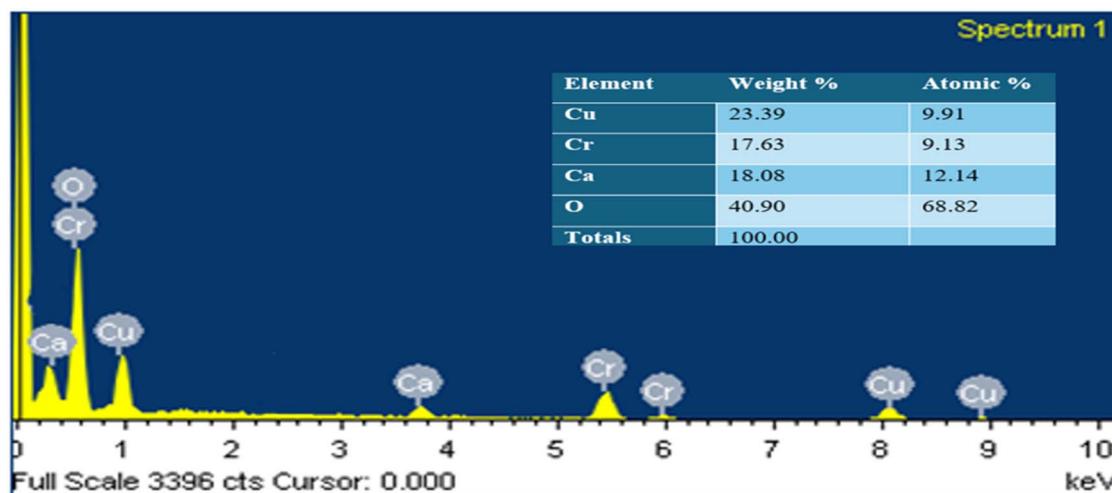

Fig. 3 SEM of the trimetallic Cu–Cr–Ca nanocatalyst.

Fig. 4 EDX plot of the trimetallic Cu–Cr–Ca nano-catalyst.

Ca nanocatalyst (Fig. 5). The FTIR spectrum shows strong bands in the 651–677 cm^{-1}, 711–738 cm^{-1}, and 853–898 cm^{-1} regions, which are assigned to the Cr–O, Ca–O, and Cu–O bending vibrations, respectively. The reported peaks predominantly belong to the metal–oxygen bond stretching vibrations and signify the preparation of Cu–Cr–Ca nanocatalyst. In a similar study of trimetallic CuO–NiO–ZnO metal oxides, the reported peaks under 1000 cm^{-1} were attributed to vibrations belonging to the metal–oxygen bond.[51] The peak at 1109 cm^{-1} is attributed to C–O stretching.

Some previous studies on metal oxides align well with our findings. For instance, in the investigation of Cr$_2$O$_3$ NPs, the peak below 1000 cm^{-1}, particularly at 839 cm^{-1}, is associated with Cr–O vibrations, which falls within our observed peak range.[52] In another work, the peaks at 711 cm^{-1} and 872 cm^{-1} in CaO NPs[53] correlate well with the respective peak bands at 711–

738 cm^{-1} and 853–898 cm^{-1} observed in our present study. The presence of Cr–O and Cu–O functional groups provides both acidic and basic active sites responsible for bifunctional roles enabling simultaneous esterification and transesterification. Ca–O facilitates methanol deprotonation resulting in nucleophilic methoxide formation because of its basic site availability, which is essential for transesterification, while the acidic site makes the triglyceride more susceptible to nucleophilic attack.

3.3 Optimization of process parameters by RSM

A four factor CCD model was employed to optimize the nano catalytic transesterification of *Phyllanthus emblica* L. oil. The response variable is biodiesel yield, which is obtained by proceeding experimental runs at the parameters given by the CCD model. A quadratic equation (eqn (2)) results in the regression analysis of the CCD model with the response
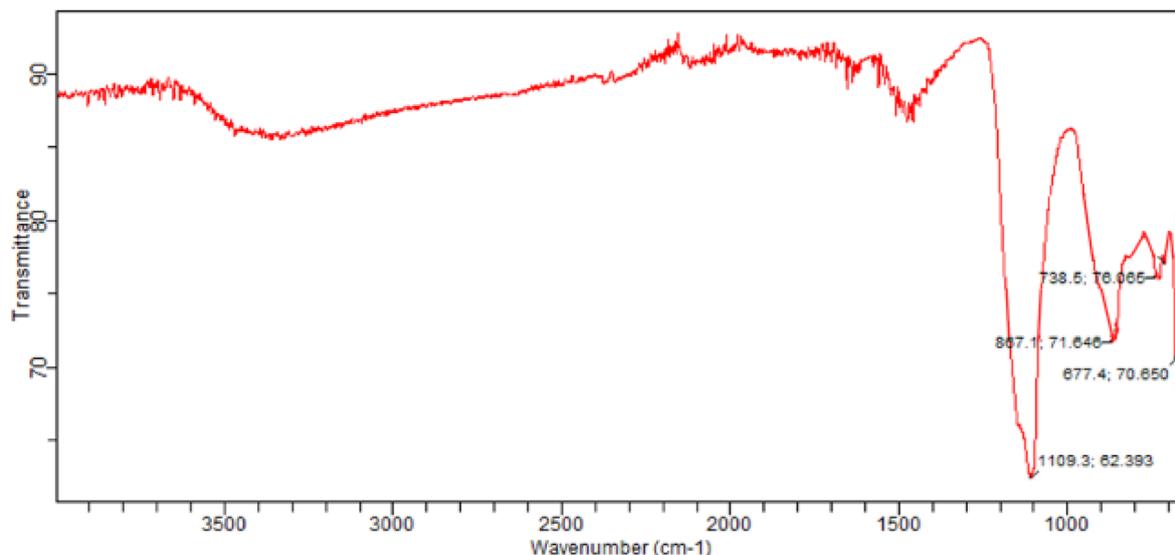

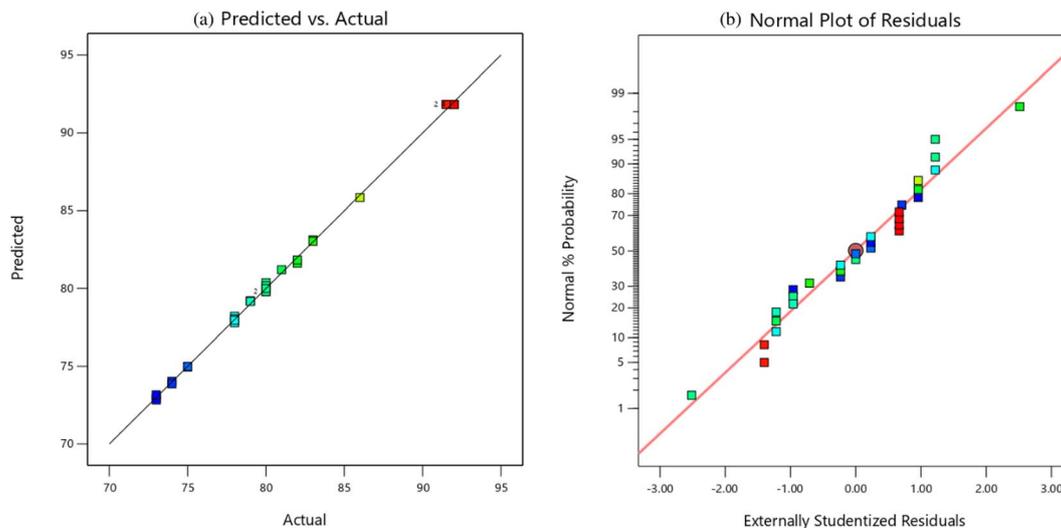**Fig. 5** FTIR spectrum of the trimetallic Cu–Cr–Ca nano-catalyst.

Fig. 6 (a) Actual *versus* predicted value plot of the amla oil transesterification optimization. (b) Normal probability plot of residuals of the amla oil transesterification optimization.

variable, which is further used to predict the FAMEs yield. The close alignment between the experimental and predicted value of *P. emblica* biodiesel yield in the actual *vs.* predicted plot shows linear relation between these two data set points (Fig. 6a). Also, the normal distribution of data in normality plot validates the ANOVA results (Fig. 6b).

Table 3 CCD-based experimental and predicted yields for amla oil transesterification

Run	Methanol : amla oil	Cu–Cr–Ca concentration (g)	Reaction temperature (°C)	Time (hours)	Response Actual value (%)	Predicted value (%)	Residual
1	9	3	85	5	92	91.83	0.1667
2	9	1	85	5	82	81.83	0.1667
3	12	4	80	4	82	81.63	0.375
4	6	2	90	6	83	83.13	−0.125
5	9	3	85	5	92	91.83	0.1667
6	6	4	90	4	80	79.79	0.2083
7	6	4	80	6	73	72.96	0.0417
8	9	3	85	7	75	75	0
9	9	3	85	5	91.5	91.83	−0.3333
10	9	3	75	5	79	79.17	−0.1667
11	15	3	85	5	73	73.17	−0.1667
12	9	3	85	5	92	91.83	0.1667
13	9	3	95	5	86	85.83	0.1667
14	12	4	90	6	78	77.96	0.0417
15	6	2	90	4	80	80.38	−0.375
16	6	2	80	6	74	74.04	−0.0417
17	12	2	90	4	80	79.79	0.2083
18	9	3	85	5	91.5	91.83	−0.3333
19	9	3	85	5	92	91.83	0.1667
20	9	5	85	5	80	80.17	−0.1667
21	6	4	90	6	78	78.04	−0.0417
22	3	3	85	5	73	72.83	0.1667
23	12	2	80	6	75	74.96	0.0417
24	12	2	80	4	78	78.21	−0.2083
25	12	2	90	6	83	83.04	−0.0417
26	9	3	85	3	80	80	0
27	12	4	80	6	74	73.88	0.125
28	6	4	80	4	81	81.21	−0.2083
29	6	2	80	4	78	77.79	0.2083
30	12	4	90	4	79	79.21	−0.2083

Predicted yield of AOMEs

$$\begin{aligned} Y = {}& 91.8333 + 0.0833333A \\ & - 0.416667B + 1.66667C - 1.25D \\ & + 5.2726e - 15AB - 0.25AC \\ & + 0.125AD - 1BC - 1.125BD \\ & + 1.625CD - 4.70833A^2 \\ & - 2.70833B^2 - 2.33333C^2 \\ & - 3.58333D^2 \end{aligned} \tag{2}$$

where A, B, C and D are the methanol-to amla oil molar ratio, Cu–Cr–Ca concentration (wt%), reaction temperature (°C), and reaction time (min), respectively. Table 3 reports the actual and predicted value of the response to CCD model.

ANOVA is employed to examine the significance of parameters in an experimental model, helping determine which variables significantly impact the response. Table 4 reports the ANOVA results of the present CCD model with the large F-value ($F_{\text{model}} = 1135.96$) and small probability value ($p < 0.0001$) indicating the strong significance of the model. The biodiesel yield is explained by the independent variables, as demonstrated by the R^2 value of 0.9991, demonstrating a strong model fit. Eleven out of fourteen model terms are significant due to the p-value < 0.0500. Furthermore, the predicted R^2 of 0.9958, which estimates how well the model can predict new data, closely aligns with the adjusted R^2 of 0.9982, which accounts for the quantity of factors in the model. This close agreement indicates that the model is neither overfitted nor underfitted, ensuring its reliability.

3.4 Influence of reaction conditions on AOMEs yield

One of the main purposes of the current study is to optimize the biodiesel production from amla oil to obtain the ideal parameter for the maximum yield. Optimizing the factors influencing biodiesel yield is essential to achieving optimal yields while minimizing by-products such as glycerol, soaps, or unreacted oils.

The influence of methanol to amla oil molar ratio on % response yield was demonstrated in Fig. 7a, with the greatest yield of 92% at a methanol to amla oil ratio of 9 : 1. Further, any deviation in ratio results in a drop in the AOMEs yield. At a 3 : 1 methanol to amla oil ratio, the yield declines to 73% while it is 85% at 15 : 1. Usually, three moles of alcohol are necessary for the transesterification of 1 mole of triglyceride but an excess of alcohol can help increase the conversion rate by shifting the equilibrium towards the product side.[16] As depicted in Fig. 7a, ratios higher than the 9 : 1 methanol to oil ratio result in a decline in AOME percentage yield, which can be associated to the flooding of the active site of the catalyst by an excess of alcohol, resulting in mitigation of conversion due to interrupted protonation of triglycerides on the active site of the catalyst.[54] Another reason could be the occurrence of counter-reactions due to excessive dilution, in accordance with Le Chatellier's principle. The ANOVA results also identify the methanol-to-oil ratio as a significant factor, emphasizing that achieving the optimal concentration is crucial for optimal yield (Table 4).

The Cu–Cr–Ca nanocatalyst dosage is an influential parameter with notable impact on AOMEs yield. The optimal AOMEs yield of 92% was obtained using 3 g of Cu–Cr–Ca. The AOMEs yield of 82% resulted from a catalyst loading of 1 g and a further increase in catalyst loading to 3 g resulted in increased biodiesel yield (92%). The increasing catalyst concentration leads to a higher number of active sites available for the reaction (Fig. 7b).[55] An increase in catalyst loading above 3 g causes a decrease in biodiesel yield (80% at 5 g loading), mainly due to slurry and soap formation as a byproducts of the catalyst and agglomeration of catalyst particles from excessive catalyst.[23] Previously, Munir et al. (2021) reported 89.42% methyl ester yield from Celastrus paniculatus Willd. oil using a trimetallic Ce–Cu–La catalyst.[16] Cu–Cr–Ca catalyzed amla oil transesterification produced a slightly higher yield of 92% at 85 °C,

Table 4 ANOVA for the quadratic model[a]

Source	Sum of squares	df	Mean square	F-Value	p-Value	
Model	1148.58	14	82.04	1135.96	<0.0001	Significant
A-methanol : amla oil	0.1667	1	0.1667	2.31	0.1495	
B-Cu–Cr–Ca concentration	4.17	1	4.17	57.69	<0.0001	
C-temperature	66.67	1	66.67	923.08	<0.0001	
D-time	37.50	1	37.50	519.23	<0.0001	
AB	0.0000	1	0.0000	0.0000	1.0000	
AC	1.0000	1	1.0000	13.85	0.0020	
AD	0.2500	1	0.2500	3.46	0.0825	
BC	16.00	1	16.00	221.54	<0.0001	
BD	20.25	1	20.25	280.38	<0.0001	
CD	42.25	1	42.25	585.00	<0.0001	
A^2	608.05	1	608.05	8419.12	<0.0001	
B^2	201.19	1	201.19	2785.71	<0.0001	
C^2	149.33	1	149.33	2067.69	<0.0001	
D^2	352.19	1	352.19	4876.48	<0.0001	
Residual	1.08	15	0.0722			
Lack of fit	0.7500	10	0.0750	1.13	0.4767	Not significant
Pure error	0.3333	5	0.0667			
Cor. total	1149.67	29				

[a] CV% = 0.3311, R^2 = 0.9991, R_{adj}^2 = 0.9982, predicted R^2 = 0.9958, Adeq. precision = 99.985.
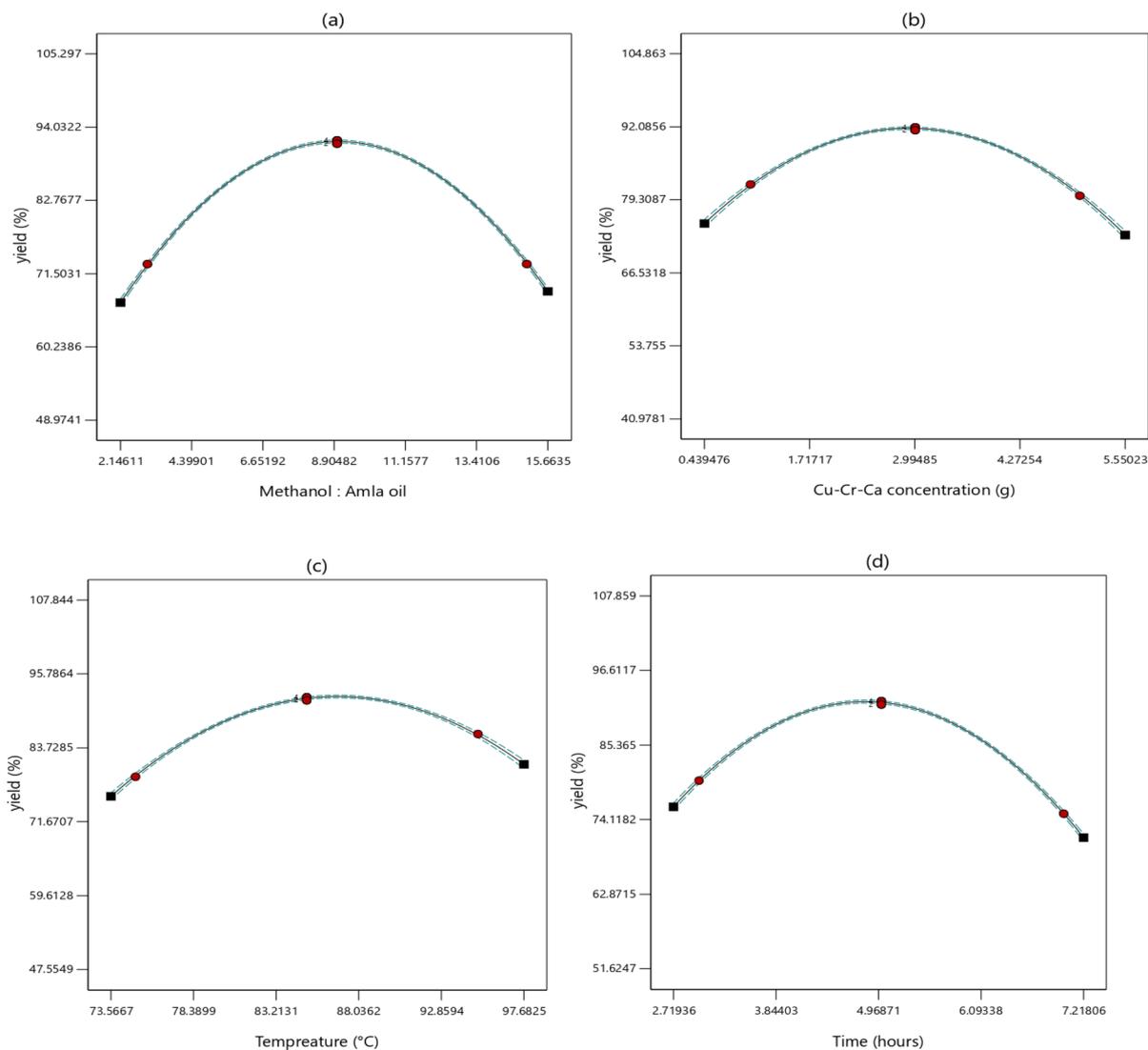
Fig. 7 (a) Effect of alcohol : oil molar ratio, (b) catalyst concentration, (c) reaction temperature, and (d) reaction time.

a lower methanol-to-oil molar ratio of 9 : 1, and 3 g of catalyst, as opposed to 12 : 1, 3.5%, and 120 °C for the Ce–Cu–La catalyst.

The reaction temperature influenced the AOMEs yield in accordance with the Arrhenius equation with an optimum yield of 92% at 85 °C (Fig. 7c). The increase in AOMEs yield from 79% at 75 °C to a maximum of 92% at 85 °C can be linked to a decrease in the viscosity of oil and mass transfer limits but any further increase in temperature resulted in a decrease in yield (86% at 95 °C), mainly attributed to the methanol vaporization at higher temperature. These results align well with the findings of Munir *et al.* (2021) and Zhang *et al.* (2020), both of which indicate that increasing temperature initially leads to an increase in % biodiesel yield within a certain range, then falls.[16,55]

The impact of reaction time on the conversion of amla oil to AOMEs is shown in Fig. 7d. The 3 h prolonged transesterification of amla oil gives a yield of 80%, which further increases to 92% at 5 h of reaction but further increments in the

reaction time results in a decrease of the AOMEs yield (75% at 7 h), mainly due to an unwanted saponification side reaction.

3D contours plots in Fig. 8a–f are used to study the interaction among the reaction variables and their combined impact on AOMEs yield. The best yield of 92% was obtained as a result of transesterification of *Phyllanthus emblica* L. oil at the optimal conditions of 9 : 1 methanol to oil ratio, 3 g of Cu–Cr–Ca, 85 °C and 5 h reaction time. Anbia *et al.* (2021) reported 90% FAMEs yield from waste cooking oil using trimetallic Ca–Mg–Al mixed metal oxide catalyst.[56] This is slightly less than the Cu–Cr–Ca catalyzed amla oil transesterification yield (92%) under comparable reaction conditions in this study.

The Cu–Cr–Ca nanocatalyst is innovative due to its trimetallic composition with greater surface area, active sites and stability against leaching resulting in better reaction kinetics and making it a reliable and sustainable option for biodiesel production from non-edible oil sources like amla.
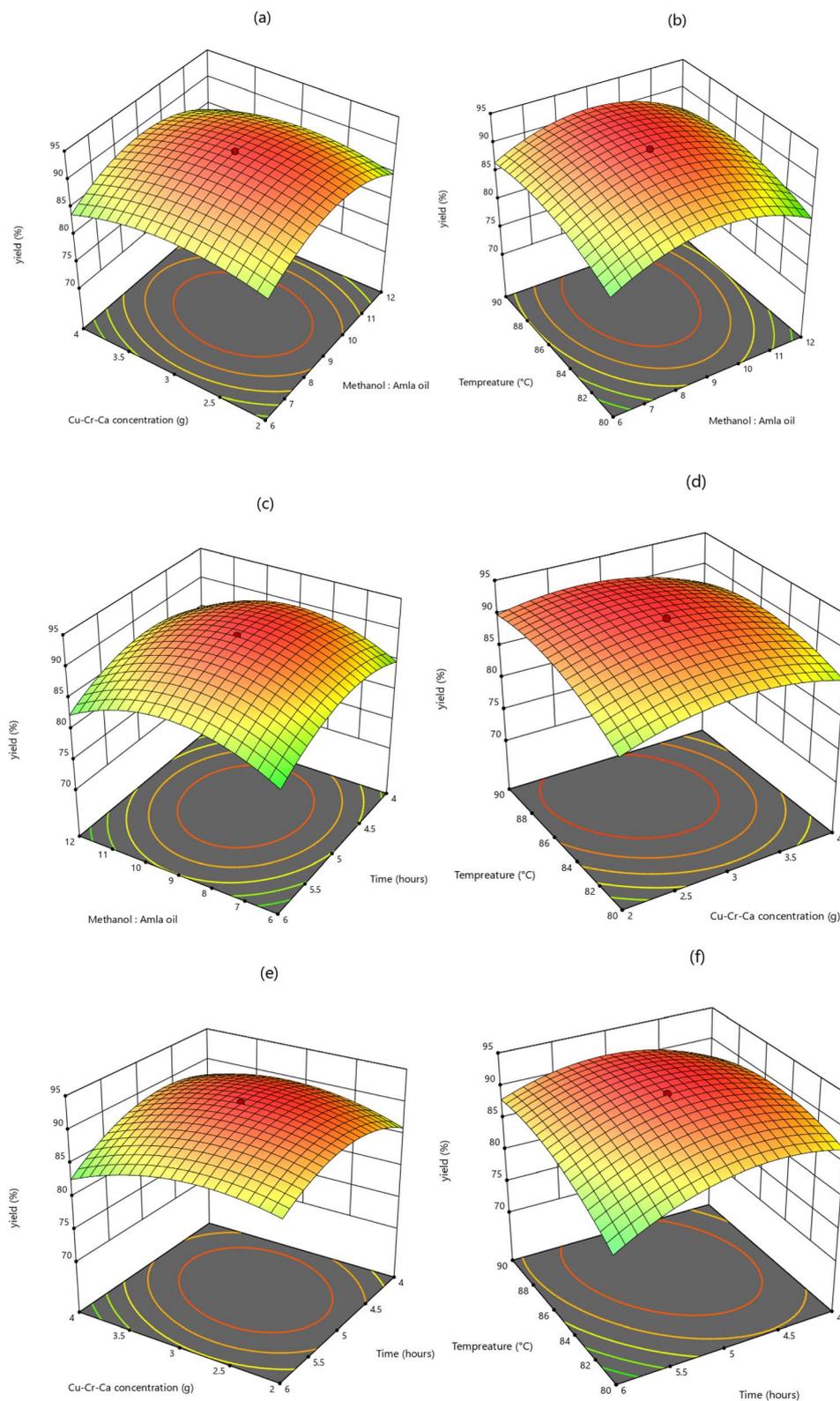
Fig. 8   3D response surface plots depicting the influence of multiple variables on the biodiesel yield.

3.5 Mechanism and synergistic role of Cu–Cr–Ca nanocatalyst in transesterification

The transesterification mechanism catalyzed by CaO, CuO, and Cr_2O_3 follows distinct, yet interrelated pathways based on their acid–base properties (Fig. 9). CaO, a strongly basic oxide, facilitates proton abstraction from methanol through its highly reactive basic site (O^{2-}) sites, generating nucleophilic methoxide ions (CH_3O^-). These methoxide ions attack the carbonyl carbon of triglycerides, forming a tetrahedral alkoxy carbonyl intermediate, which subsequently decomposes to yield biodiesel and a diglyceride, continuing the reaction cycle until full conversion to monoglycerides and glycerol.[34] In contrast, CuO,
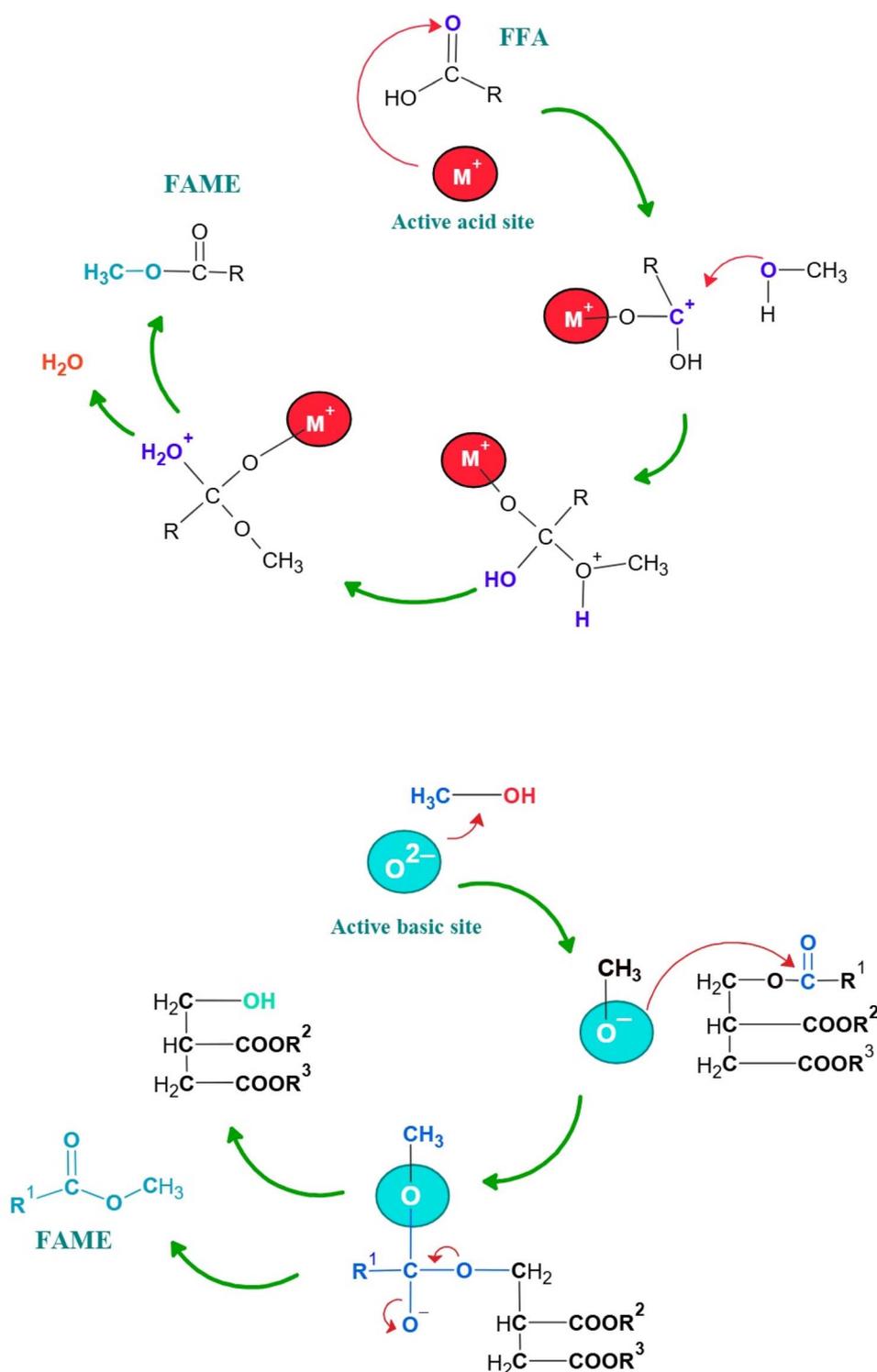

Fig. 9 Schematic of the bifunctional heterogeneous acid–base catalyzed transesterification mechanism.[34]

RSC Advances

a weakly amphoteric oxide, and Cr_2O_3, a fully amphoteric oxide, exhibit bifunctional catalytic behaviour due to the presence of Lewis acidic (Cu^{2+}/Cr^{3+}) and basic (O^{2-}) sites. Their basic sites deprotonate methanol, generating methoxide ions, which attack the carbonyl carbon of triglycerides, forming a tetrahedral alkoxy carbonyl intermediate, which subsequently undergo C–O bond cleavage to yield biodiesel. Meanwhile, their Lewis acid sites facilitate esterification by adsorbing FFAs, forming a carbocation intermediate that undergoes nucleophilic attack by methanol. The resulting tetrahedral species then breaks the O–H bond and produces a FAME molecule.[34]

The reaction takes place on the active sites of nanoparticles, which means that the larger the number of sites, the greater the reaction rate. The catalytic active sites are basically surface atoms of ternary metal oxides which rise with decreasing particle size. The reduced size also increases surface atoms in corners and edges which are more active than atoms in planes, resulting in more enhanced catalytic activity. A large number of surface atoms remain weakly connected to the lattice due to the extremely high curvature of very small particles, enhancing their reactivity.[57] Therefore, the surface atoms of these particles are considered to be in a state of physical instability, extremely active, and prone to various chemical reactions. As a result, they have very high surface energies. When particles are small, diffusion forces can push the product away from the surface, speeding up chemical reactions. The synthesized Cu–Cr–Ca nanocatalyst has an average particle size of 25.67 nm as confirmed by XRD analysis, which is significantly smaller than conventional catalysts like bulk CaO. This reduction in size enhances the catalytic activity by increasing the number of active sites available for reactant adsorption and reducing the reaction activation energy, resulting in accelerated transesterification rate.

In comparison to traditional catalysts, nanocatalysts also make it possible to produce biodiesel at relative normal conditions like lower reaction temperatures and methanol to oil molar ratio. Zhang et al. (2020) reported a palm oil biodiesel yield of 98% using ternary oxide $SrO–CaOAl_2O_3$ at 65 °C for 3 h with a methanol to oil ratio of 18 : 1 and catalyst concentration of 7.5 wt%.[55] Lee et al. (2016) studied the heterogeneous alkaline based mixed metal oxides CaO–MgO, CaO–ZnO, CaO–La_2O_3, and MgO–ZnO as catalysts for biodiesel production from crude jatropha oil. CaO–ZnO gives the highest yield of 94% under the optimal conditions of 120 °C, 25 : 1 methanol to oil ratio, 3 wt% catalyst concentration and 3 h reaction duration.[38] Ullah et al. (2015) reported 76.61% amla oil biodiesel yield at 1% CaO under a 2 h reaction time, 1 : 6 oil to methanol ratio and 600 rpm stirring rate.[33] The comparative analysis of the present study with previous biodiesel production studies is summarized in Table 5. The present work achieved a 92% amla biodiesel yield at a 9 : 1 methanol-to-oil ratio, 3 g of Cu–Cr–Ca catalyst, 85 °C, and 5 h reaction time, outperforming the 76.61% yield reported by Ullah et al. (2015) using simple CaO, demonstrating improved efficiency under moderate reaction conditions.[33] This improvement can be linked to the synergistic effect of CuO, Cr_2O_3 and CaO nanocatalysts. The strongly basic CaO, facilitates an efficient heterogeneous base-catalyzed transesterification. Meanwhile, amphoteric transition metal oxide nanoparticles (NPs) of CuO and Cr_2O_3 carry out transesterification and esterification reactions simultaneously.

The presence of Lewis acid and Lewis base sites in CuO and Cr_2O_3 enhance catalytic efficiency along with effective conversion of high FFA oils. Cr_2O_3 exhibits redox properties that help maintain an active surface, allowing the catalyst to regenerate over multiple reaction cycles. Meanwhile, CuO facilitates excellent electron transfer, reducing the activation energy for transesterification and enhancing reaction efficiency. Transition metal oxide NPs exhibit superior water tolerance compared with group 1 and group 2 metal oxides, preventing no soap formation during the reaction.[38] This also improves biodiesel

Table 5 Summary of various catalysts used for biodiesel production from different oil sources under optimized reaction conditions

Catalyst	Oil source	Methanol/oil ratio	Catalyst amount	Temperature (°C)	Time (h)	Yield (%)	Reference
Cr–Al mixed oxide	*Scenedesmus obliquus* (microalgae)	20 : 1	15%	80	—	98.28	58
CuO nanoparticles	*Calotropis gigantea* seed oil	9 : 1	0.74 wt%	80	1.75	90	59
$SrO–CaO–Al_2O_3$	Palm oil	18 : 1	7.5 wt%	65	3	98.16	55
CaO (from calcium nitrate and snail shell)	Soybean oil	12 : 1	8 wt%	65	6	96	60
GO@ZrO_2–SrO nanocomposite	Waste cooking oil	4 : 1	—	120	1.5	91	61
HNTs–La/Ca	Palm oil	18 : 1	7 wt%	150	2	97.5	62
Fe–Co–Ni on bentonite	Palm kernel oil	10 : 1	5%	55	2	95.2	32
CaO–ZnO	Jatropha oil	25 : 1	3 wt%	120	3	94	38
CaO (from watermelon peel extract)	Soybean oil	20 : 1	8 wt%	65	2.5	96.2	63
DMC/activated charcoal	Amla oil	6 : 1	1.5 wt%	80	—	89	45
CaO/Fe–Ca	Amla oil	6 : 1	1% CaO/2.5% Fe–Ca	—	2	76.61/90.31	33
Cu–Cr–Ca oxides NPs	Amla oil	9 : 1	3 g	85	5	92	Present study

yield by minimizing side reactions and by-product formation, ultimately ensuring easier product separation at the end of the reaction. Consequently, the Cu–Cr–Ca oxide trimetallic nano-catalyst in the present study achieved the highest given yield of amla biodiesel compared with previous studies.

3.6 GC-MS characterization of amla biodiesel

The biodiesel chemical composition plays an important role in assessing its quality and appropriateness for different applications. GC-MS was employed in this study to profile and characterize the nature and quantity of chemical constituents of biodiesel derived from *Phyllanthus emblica* L. oil. Ten distinct peaks were detected in the GC-MS chromatogram (Fig. 10), each indicative of a specific fatty acid methyl ester present in the amla oil-derived biodiesel. Ten identified fatty acid methyl esters are categorized into saturated fatty acids (SFAs), comprising of ethyl palmitate ($C_{18:0}$), dioctyl phthalate ($C_{23:0}$), and unsaturated fatty acids (UFAs) including methyl linoleate ($C_{19:2}$), *trans*-vaccenic acid methyl ester ($C_{19:1}$), linoleic acid ethyl ester ($C_{20:2}$), ethyl oleate ($C_{20:1}$), methyl ricinoleate ($C_{19:1}$),

Fig. 10 GC-MS chromatogram showing fatty acid composition of the AOMEs (*Phyllanthus emblica* L. biodiesel).

ethyl ricinoleate ($C_{20:1}$), methyl erucate ($C_{23:1}$) and ethyl erucate ($C_{24:1}$). Table 6 presents the retention times and relative percent composition of the detected ten identified methyl esters. The *trans*-vaccenic acid, methyl ester was the most abundant constituent comprising 20.01% of the total identified esters. Furthermore, unsaturated fatty acids (UFA) dominate the composition at 85.98%, while saturated fatty acids (SFA) collectively represent 14.03%.

3.7 FTIR analysis of amla oil and amla biodiesel

The FTIR spectroscopic analysis of amla seed oil and nano-catalyzed amla biodiesel provided a comprehensive insight of the present functional groups and the chemical transformations that occurred during the transesterification process. FTIR spectra are ranged from 650 to 4000 cm^{-1}, as depicted in Fig. 11a and b. In amla oil spectra (Fig. 11a), the double band at 2853 cm^{-1} and 2923 cm^{-1} is due to $-CH_2$ symmetric and asymmetric stretching vibrations, respectively and a strong intensity peak at 1743 cm^{-1} identifies $-C=O$ stretching. The transmittance between 1097 cm^{-1} and 1159 cm^{-1} resonate with $-C-O$ stretching while the peak at 1375 cm^{-1} is attributed to the $O-CH_2$ glyceride group and both regions are not present in the biodiesel spectrum. The spectrum of AOBD shows an intense absorption peak at 1734 cm^{-1} and 1739 cm^{-1} due to $-C=O$ stretching in esters (Fig. 11b). The peaks at 1037 cm^{-1} and 1096 cm^{-1} are not present in oil and represent the $-C-O$ stretching mode of the C–OH group of esters. The bending peaks at 797, 1457, 2855, 2920 cm^{-1} are associated with CH_3 and CH_2 stretching, which indicate existence of methyl and methylene units in the biodiesel. The removal of glycerides, formation of ester groups and the introduction of methyl groups are the primary transformations showing significant chemical change and conversion of *P. emblica* seed oil to biodiesel.

3.8 Fuel properties of AOMEs

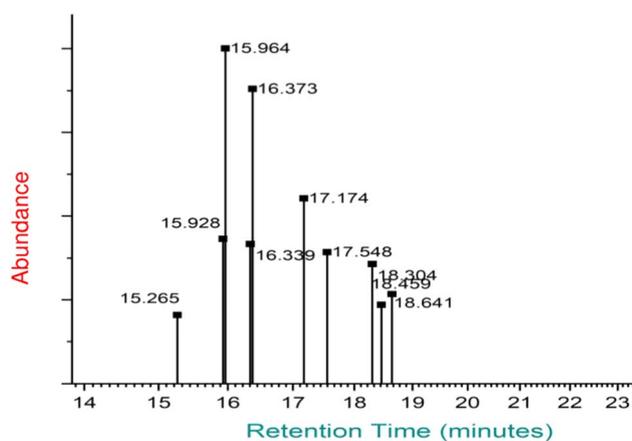To evaluate the quality and potential of synthesized amla oil biodiesel as a fuel, physico-chemical characteristics of

Table 6 Quantification of FAs in the amla oil biodiesel using GC-MS chromatography

| Sr. no.	Retention time (min)	Compound found	Common name	Molecular formula	Fatty acid	Area (%)
1	15.265	Hexadecanoic acid, ethyl ester	Ethyl palmitate	$C_{18}H_{36}O_2$	$C_{18:0}$	4.09
2	15.928	9,12-Octadecadienoic acid (Z,Z), methyl ester	Methyl linoleate	$C_{19}H_{34}O_2$	$C_{19:2}$	8.65
3	15.964	11-Octadecenoic acid, methyl ester	*Trans*-vaccenic acid, methyl ester	$C_{19}H_{36}O_2$	$C_{19:1}$	20.01
4	16.339	Linoleic acid ethyl ester	Ethyl linoleate	$C_{20}H_{36}O_2$	$C_{20:2}$	8.34
5	16.373	Ethyl oleate	Ethyl oleate	$C_{20}H_{38}O_2$	$C_{20:1}$	17.6
6	17.174	9-Octadecenoic acid, 12-hydroxy, methyl ester, [R-(Z)]	Methyl ricinoleate	$C_{19}H_{36}O_3$	$C_{19:1}$	11.05
7	17.548	9-Octadecenoic acid, 12-hydroxy, ethyl ester, [R-(Z)]	Ethyl ricinoleate	$C_{20}H_{38}O_3$	$C_{20:1}$	7.85
8	18.304	13-Docosenoic acid, methyl ester, (Z)	Methyl erucate	$C_{23}H_{44}O_2$	$C_{23:1}$	7.14
9	18.459	Bis(2-ethylhexyl) phthalate	Dioctyl phthalate	$C_{24}H_{38}O_4$	$C_{23:0}$	4.7
10	18.641	Ethyl 13-docosenoate (ethyl erucate)	Ethyl erucate	$C_{24}H_{46}O_2$	$C_{24:1}$	5.34
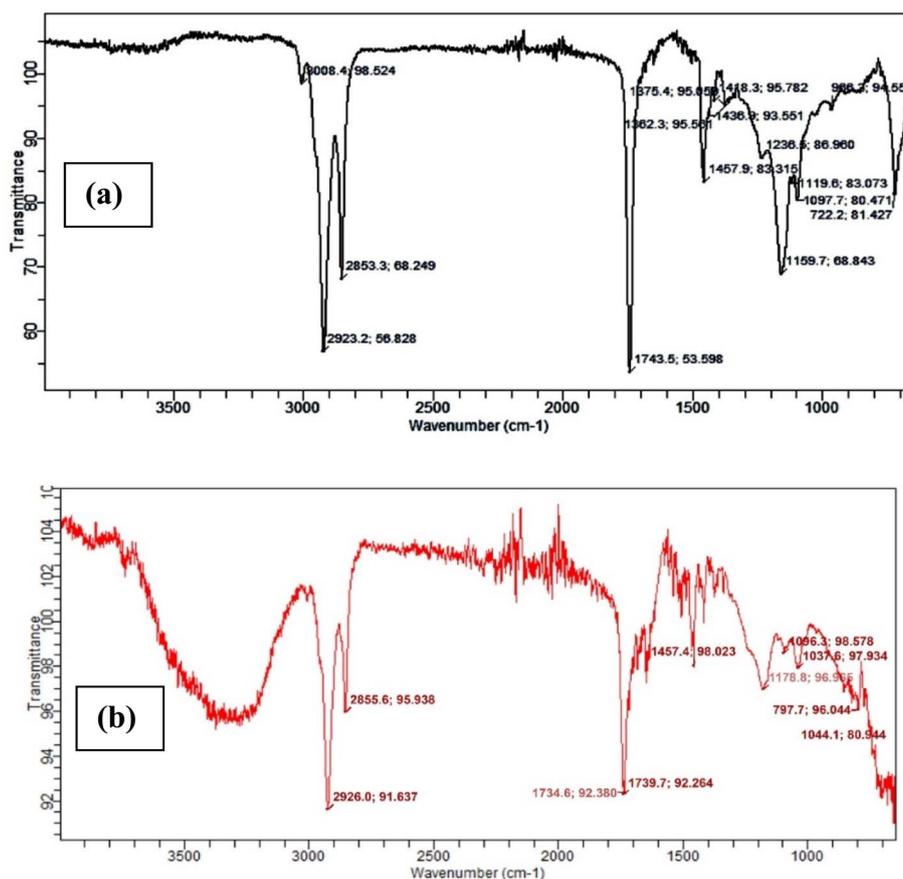
Fig. 11 FTIR spectrum of (a) amla oil and (b) amla oil biodiesel (AOMEs).

synthesized AOMEs were determined and further evaluated against the ASTM A6751 standards. The density of AOMEs was determined to be 0.88 ± 0.03 g cm^{-3}, which falls within the ASTM D6751 limits of 0.87–0.90 g cm^{-3}. The kinematic viscosity, an essential parameter which impacts the fuel flow, atomization and injection for the amla biodiesel is determined to be 4.21 ± 0.27 mm^2 s^{-1}, which is within the specified range of 1.9–6.0 mm^2 s^{-1}. Ullah *et al.* (2015) observed a slightly higher kinematic viscosity of 4.64 mm^2 s^{-1} for amla biodiesel indicating that different catalysts for transesterification influence fuel properties.[33] The kinematic viscosity and density of FAMEs/biodiesel are highly sensitive to temperature and composition. Biodiesel is generally denser and has higher kinematic viscosity compared with conventional fuel due to long chain fatty acid esters, cyclic compounds and multiple bonds.[64] One of the primary aims of employing transesterification for biodiesel synthesis is to lower the density and viscosity of oil to make a suitable fuel.

The flash point determined for the present AOMEs is 158 ± 4 °C, which satisfies the minimum requirement of 130 °C necessary for the safety purpose.[39] The flash point is a vital indicator of the volatility of biodiesel, which is crucial for ensuring safe transportation and storage. A higher flash point indicates a higher temperature requirement for ignition, reducing the risk of accidental ignition during handling or transit. The cold filter plugging point (CFPP) is a cold flow property that reflects the lowest temperature at which fuel can pass through a filter without clogging. For the AOMEs, the CFPP value is -3 ± 0.02 °C (Table 7), which shows moderate cold weather operability. The pour point is the temperature at which fuel starts to flow under gravity and the cloud point is the temperature at which wax crystal begin to form. Their measured values for the AOMEs are -1.0 ± 1.5 °C and 2.0 ± 0.7 °C, respectively. The easy crystallization of fuel can lead to bad engine performance due to blocking of fuel filters. Agglomerates formed in fuel due to crystallization cease fuel flow and the high saturated fatty acid proportion is usually responsible for the elevated cloud and pour point.[23] The transesterification process significantly reduces the pour and cloud point, resulting in improved fuel quality. All of the physico-chemical characteristics evaluated for the AOMEs are in close accord with the

Table 7 Fuel characteristics of AOMEs relative to the biodiesel standards

Parameters	AOMEs	ASTM D6751
Density (g cm^{-3})	0.88 ± 0.03	0.87–0.90
Cold filter plugging point (°C)	-3 ± 0.02	—
Pour point (°C)	-1.0 ± 1.5	Unspecified
Flash point (°C)	158 ± 4	Minimum 130
Cloud point (°C)	2.0 ± 0.7	Unspecified
Kinematic viscosity (mm^2 s^{-1})	4.21 ± 0.27	1.9–6.0

ASTM standards, suggesting excellent quality of the produced biodiesel and supporting prospective biodiesel applications.

4 Conclusion

The current research outlines the nanocatalytic transesterification of *Phyllanthus emblica* L. oil and its optimization using central composite response design. The trimetallic Cu–Cr–Ca nanocatalyst is synthesized using a coprecipitation method, structurally characterized and then employed for the transesterification of amla oil. A 5 h reaction time at 85 °C, with 3 g of Cu–Cr–Ca loading and 9 : 1 methanol-to-oil molar ratio is determined as the optimum parameters for the best amla oil biodiesel (AOBD) yield of 92%. *Trans*-vaccenic acid, methyl ester with 20.01% of the total composition, is the most predominant constituent as evidenced by GC-MS analysis of AOBD. The fuel characteristics are in close agreement with ASTM standards, giving an acceptable 158 ± 4 °C flash point and 4.21 ± 0.27 mm^2 s^{-1} kinematic viscosity. These findings encourage further research in nanocatalytic transesterification and optimization using different feedstock sources and nanocatalysts for more cost-effective biodiesel production.

Abbreviations

AOMEs	Amla oil methyl esters
ANOVA	Analysis of variance
AOBD	Amla oil biodiesel
ASTM	American society for testing materials
Cu–Cr–Ca	Copper–chromium–calcium
CCD	Central composite design
EDX	Energy dispersive diffractometry
FAMEs	Fatty acid methyl esters
FFA	Free fatty acid
FTIR	Fourier transform infra-red
GC-MS	Gas chromatography mass spectrometry
IV	Iodine number
M	Molarity
N	Normality
NPs	Nanoparticles
POV	Peroxide value
R^2	Coefficient of determination
RSM	Response surface methodology
SEM	Surface electron microscopy
Vol	Volume
XRD	X-ray diffractometry

Data availability

The authors confirm that the data supporting the findings of this study are available within the article and its ESI.†

Author contributions

Humaira Kanwal: conceptualization, methodology, investigation, and writing original draft. Ahsan Tanvir: formal analysis, methodology, investigation, and writing original draft. Farooq Anwar: conceptualization, supervision, funding acquisition, and review and editing. Muhammad Waseem Mumtaz: supervision and technical refining. Syed Hussain Imam Abidi: project administration.

Conflicts of interest

The authors declare no conflicts of interest related to this research.

References

1 C. Liu and Q. Li, Air pollution, global warming and difficulties to replace fossil fuel with renewable energy, *Atmos. Clim. Sci.*, 2023, **13**(4), 526–538.

2 A. I. Osman, M. Nasr, M. Farghali, A. K. Rashwan, A. Abdelkader, A. A. Al-Muhtaseb, I. Ihara and D. W. Rooney, Optimizing biodiesel production from waste with computational chemistry, machine learning and policy insights: a review, *Environ. Chem. Lett.*, 2024, **22**(3), 1005–1071.

3 L. Chen, G. Msigwa, M. Yang, A. I. Osman, S. Fawzy, D. W. Rooney and P. S. Yap, Strategies to achieve a carbon neutral society: a review, *Environ. Chem. Lett.*, 2022, **20**(4), 2277–2310.

4 A. S. Silitonga, M. H. Hassan, H. C. Ong and F. Kusumo, Analysis of the performance, emission and combustion characteristics of a turbocharged diesel engine fuelled with *Jatropha curcas* biodiesel-diesel blends using kernel-based extreme learning machine, *Environ. Sci. Pollut. Res.*, 2017, **24**, 25383–25405.

5 O. Ogunkunle and N. A. Ahmed, Overview of biodiesel combustion in mitigating the adverse impacts of engine emissions on the sustainable human–environment scenario, *Sustainability*, 2021, **13**(10), 5465.

6 S. Mahapatra, D. Kumar, B. Singh and P. K. Sachan, Biofuels and their sources of production: a review on cleaner sustainable alternative against conventional fuel, in the framework of the food and energy nexus, *Energy Nexus*, 2021, **4**, 100036.

7 K. N. Krishnamurthy, S. N. Sridhara and C. A. Kumar, Optimization and kinetic study of biodiesel production from *Hydnocarpus wightiana* oil and dairy waste scum using snail shell CaO nano catalyst, *Renew. Energy*, 2020, **146**, 280–296.

8 A. Röttig, L. Wenning, D. Bröker and A. Steinbüchel, Fatty acid alkyl esters: perspectives for production of alternative biofuels, *Appl. Microbiol. Biotechnol.*, 2010, **85**, 1713–1733.

9 A. E. Atabani, A. S. Silitonga, I. A. Badruddin, T. M. Mahlia, H. Masjuki and S. Mekhilef, A comprehensive review on biodiesel as an alternative energy resource and its characteristics, *Renewable Sustainable Energy Rev.*, 2012, **16**(4), 2070–2093.

10 W. Parawira, Biodiesel production from *Jatropha curcas*: a review, *Sci. Res. Essays*, 2010, **5**(14), 1796–1808.

11 E. M. Shahid and Y. Jamal, Production of biodiesel: a technical review, *Renewable Sustainable Energy Rev.*, 2011, **15**(9), 4732–4745.

12 L. Rominiyi, B. Adaramola, J. F. Eiche, O. T. Oginni, D. V. Ewere and T. O. Oni, Tranesterification and Comparative Analysis of Bio Diesel Production Using *Blighia Sapida* (Ackee Seed) as Substrate, *Key Eng. Mater.*, 2024, **974**, 123–131.

13 F. Kusumo, T. M. Mahlia, A. H. Shamsuddin, A. R. Ahmad, A. S. Silitonga, S. Dharma, M. Mofijur, F. Ideris, H. C. Ong, R. Sebayang and J. Milano, Optimisation of biodiesel production from mixed *Sterculia foetida* and rice bran oil, *Int. J. Ambient Energy*, 2022, **43**(1), 4380–4390.

14 S. Nasreen, H. Liu, L. A. Qureshi, Z. Sissou, I. Lukic and D. Skala, Cerium–manganese oxide as catalyst for transesterification of soybean oil with subcritical methanol, *Fuel Process. Technol.*, 2016, **148**, 76–84.

15 S. Nasreen, M. Nafees, M. M. Jaffar, L. A. Qurashi and S. Tabraiz, Comparison and effect of Cinder supported with manganese and lanthanum oxide for biodiesel production, *Int. J. Hydrogen Energy*, 2017, **42**(29), 18389–18396.

16 M. Munir, M. Ahmad, M. Mubashir, S. Asif, A. Waseem, A. Mukhtar, S. Saqib, H. S. Munawaroh, M. K. Lam, K. S. Khoo and A. Bokhari, A practical approach for synthesis of biodiesel *via* non-edible seeds oils using trimetallic based montmorillonite nano-catalyst, *Bioresour. Technol.*, 2021, **328**, 124859.

17 Y. L. Chu, S. J. Young, C. J. Liu, S. Arya and T. T. Chu, Enhanced UV-Sensing Performances of 2-D Pd/ZnO Nanosheet Photodetectors through Inexpensive Photochemical Synthesis at Room Temperature and Their Humidity Applications, *ACS Appl. Electron. Mater.*, 2025, **7**(1), 129–142.

18 B. Padha, Z. Ahmed, S. Dutta, A. Pandey, N. Padha, M. Tomar, A. Sharma, I. Yadav and S. Arya, Ultrasensitive NO_2 gas detection using ALD-grown ZnO-SiO_2/Si thin film-based UV sensors, *J. Alloys Compd.*, 2025, **1010**, 177673.

19 R. Khajuria, A. Singh, M. U. Rather, A. Sharma, P. Angotra, A. K. Sundramoorthy, S. Dixit, N. I. Vatin and S. Arya, Elucidating the structural, morphological and optical properties of chalcogenide glasses within antimony-tin-selenium ternary system, *Appl. Phys. A: Mater. Sci. Process.*, 2024, **130**(10), 711.

20 P. Mahajan, A. Singh, R. Datt, W. C. Tsoi, V. Gupta and S. Arya, Synthesis and characterization of $NaYF_4$:Pr^{3+}@$NaYF_4$:Eu^{3+} core@shell nanoparticles as down-conversion material for organic solar cells application, *Eur. Phys. J. Plus*, 2024, **139**(2), 183.

21 M. D. Madhuwantha, H. Galagedara, Y. Y. Kannangara, S. Karunarathne, M. M. M. G. P. G. Mantilaka, H. C. S. Perera and W. S. L. Wijesinghe, Low-cost ZnO incorporated carbonized nitrile butadiene rubber (NBR) as a relative humidity monitoring sensor, *Mater. Sci. Eng., B*, 2023, **298**, 116862.

22 A. Ahmed, S. Arora, S. Rasgotra, A. Dubey, A. Singh, R. Singh, B. Padha, S. Dixit, N. I. Vatin and S. Arya, Synthesis and characterization of low-density polyethylene (LDPE) bubble wrap-derived reduced graphene oxide for triboelectric nanogenerator electrodes, *Mater. Sci. Eng., B*, 2025, **311**, 117828.

23 S. Bano, A. S. Ganie, S. Sultana, S. Sabir and M. Z. Khan, Fabrication and optimization of nanocatalyst for biodiesel production: an overview, *Front. Energy Res.*, 2020, **8**, 579014.

24 H. Fukuda, A. Kondo and H. Noda, Biodiesel fuel production by transesterification of oils, *J. Biosci. Bioeng.*, 2001, **92**(5), 405–416.

25 V. Polshettiwar and R. S. Varma, Green chemistry by nano-catalysis, *Green Chem.*, 2010, **12**(5), 743–754.

26 G. Allaedini, S. M. Tasirin and P. Aminayi, Synthesis of Fe–Ni–Ce trimetallic catalyst nanoparticles *via* impregnation and co-precipitation and their application to dye degradation, *Chem. Pap.*, 2016, **70**(2), 231–242.

27 S. Niju, F. R. Raj, C. Anushya and M. Balajii, Optimization of acid catalyzed esterification and mixed metal oxide catalyzed transesterification for biodiesel production from *Moringa oleifera* oil, *Green Process. Synth.*, 2019, **8**(1), 756–775.

28 J. Gardy, A. Osatiashtiani, O. Céspedes, A. Hassanpour, X. Lai, A. F. Lee, K. Wilson and M. Rehan, A magnetically separable SO_4/Fe-Al-TiO_2 solid acid catalyst for biodiesel production from waste cooking oil, *Appl. Catal., B*, 2018, **234**, 268–278.

29 M. A. Bezerra, R. E. Santelli, E. P. Oliveira, L. S. Villar and L. A. Escaleira, Response surface methodology (RSM) as a tool for optimization in analytical chemistry, *Talanta*, 2008, **76**(5), 965–977.

30 N. I. Mohammed, N. A. Kabbashi, M. Z. Alam and M. E. Mirghani, Optimization of Jatropha biodiesel production by response surface methodology, *Green Sustainable Chem.*, 2021, **11**(1), 23–37.

31 W. N. Omar and N. A. Amin, Optimization of heterogeneous biodiesel production from waste cooking palm oil *via* response surface methodology, *Biomass Bioenergy*, 2011, **35**(3), 1329–1338.

32 A. F. Alade, A. T. Latifat, M. S. Ishola, M. I. Alhassan, S. H. Bamidele, A. E. Olawale and O. S. Samuel, Heterogeneous catalysis using bentonite-supported fe-co-ni trimetallic nanoparticles, *J. Eng. Stud. Res.*, 2021, **27**(3), 7–19.

33 K. Ullah, M. Ahmad, F. A. Qureshi, R. Qamar, V. K. Sharma, S. Sultana and M. Zafar, Synthesis and characterization of biodiesel from aamla oil: a promoting non-edible oil source for bioenergy industry, *Fuel Process. Technol.*, 2015, **133**, 173–182.

34 D. Marinković and S. Pavlović, Recent advances in waste-based and natural zeolitic catalytic materials for biodiesel production, *Hem. Ind.*, 2023, **77**(1), 5–38.

35 M. Kouzu and J. S. Hidaka, Transesterification of vegetable oil into biodiesel catalyzed by CaO: a review, *Fuel*, 2012, **93**, 1–2.

36 A. Anantapinitwatna, K. Ngaosuwan, W. Kiatkittipong, D. Wongsawaeng, A. Anantpinijwatna, A. T. Quitain and S. Assabumrungrat, Water influence on the kinetics of transesterification using CaO catalyst to produce biodiesel, *Fuel*, 2021, **296**, 120653.

37 D. M. Marinković, M. V. Stanković, A. V. Veličković, J. M. Avramović, M. R. Miladinović, O. O. Stamenković, V. B. Veljković and D. M. Jovanović, Calcium oxide as a promising heterogeneous catalyst for biodiesel production: current state and perspectives, *Renewable Sustainable Energy Rev.*, 2016, **56**, 1387–1408.

38 H. V. Lee, J. C. Juan, T. Y. Yun Hin and H. C. Ong, Environment-friendly heterogeneous alkaline-based mixed metal oxide catalysts for biodiesel production, *Energies*, 2016, **9**(8), 611.

39 U. Rashid and F. Anwar, Production of biodiesel through optimized alkaline-catalyzed transesterification of rapeseed oil, *Fuel*, 2008, **87**(3), 265–273.

40 F. Anwar, M. Tariq, J. Nisar, G. Ali and H. Kanwal, Optimization of biodiesel yield from non-food karanja seed oil: characterization and assessment of fuel properties, *Sustainable Chemistry for the Environment*, 2023, **3**, 100035.

41 V. Mandari and S. K. Devarai, Biodiesel production using homogeneous, heterogeneous, and enzyme catalysts *via* transesterification and esterification reactions: a critical review, *BioEnergy Res.*, 2022, **15**(2), 935–961.

42 H. Li, P. Lv, Z. Wang, C. Miao and Z. Yuan, Biodiesel continuous esterification process experimental study and equipment design, *Biomass Convers. Biorefin.*, 2021, **11**, 3053–3060.

43 U. Rashid, S. G. Bhatti, T. M. Ansari, R. Yunus and M. Ibrahim, Biodiesel production from *Cannabis sativa* oil from Pakistan, *Energy Sources, Part A*, 2016, **38**(6), 865–875.

44 N. Manojkumar, C. Muthukumaran and G. Sharmila, A comprehensive review on the application of response surface methodology for optimization of biodiesel production using different oil sources, *J. King Saud Univ., Eng. Sci.*, 2022, **34**(3), 198–208.

45 V. Sunil, A. V. Manigandan, K. Cholapandian and P. Dhasarathan, *Production of biodiesel from Phyllanthus emblica seeds using activated charcoal as heterogeneous catalyst*, Res. Sq., 2022, DOI: 10.21203/rs.3.rs-2131146/v1.

46 V. Jadhav, A. Bhagare, S. Wahab, D. Lokhande, C. Vaidya, A. Dhayagude, M. Khalid, J. Aher, A. Mezni and M. Dutta, Green synthesized calcium oxide nanoparticles (CaO NPs) using leaves aqueous extract of *Moringa oleifera* and evaluation of their antibacterial activities, *J. Nanomater.*, 2022, **2022**(1), 9047507.

47 S. A. David, A. Doss and R. P. Pole, Biosynthesis of chromium oxide nanoparticles by *Momordica charantia* leaf extract: characterization and their antibacterial activities, *Res. Surf. Interfaces*, 2023, **11**, 100120.

48 M. B. Mobarak, M. S. Hossain, F. Chowdhury and S. Ahmed, Synthesis and characterization of CuO nanoparticles utilizing waste fish scale and exploitation of XRD peak profile analysis for approximating the structural parameters, *Arabian J. Chem.*, 2022, **15**(10), 104117.

49 Z. Vaseghi, O. Tavakoli and A. Nematollahzadeh, Rapid biosynthesis of novel Cu/Cr/Ni trimetallic oxide nanoparticles with antimicrobial activity, *J. Environ. Chem. Eng.*, 2018, **6**(2), 1898–1911.

50 G. Yasmeen, S. Hussain, A. Tajammal, Z. Mustafa, M. Sagir, M. Shahid, M. Ibrar, Z. M. Elqahtani and M. Iqbal, Green synthesis of Cr_2O_3 nanoparticles by *Cassia fistula*, their electrochemical and antibacterial potential, *Arabian J. Chem.*, 2023, **16**(8), 104912.

51 M. J. Uddin, M. S. Yeasmin, A. A. Muzahid, M. M. Rahman, G. M. Rana, T. A. Chowdhury, M. Al-Amin, M. K. Wakib and S. H. Begum, Morphostructural studies of pure and mixed metal oxide nanoparticles of Cu with Ni and Zn, *Heliyon*, 2024, **10**(9), e30544.

52 A. Bumajdad, S. Al-Ghareeb, M. Madkour and F. A. Sagheer, Non-noble, efficient catalyst of unsupported α-Cr_2O_3 nanoparticles for low temperature CO Oxidation, *Sci. Rep.*, 2017, **7**(1), 14788.

53 W. C. Ulakpa, C. Aseibichin, O. A. Chimezie, A. A. Olaseinde, E. Odeworitse, E. Onoriode and I. M. Adaeze, Nano-CaO as a heterogeneous catalyst for biodiesel synthesis by transesterification of Jatropha oil, *J. Trace Elem. Min.*, 2024, **9**, 100183.

54 Y. Zhang, W. T. Wong and K. F. Yung, One-step production of biodiesel from rice bran oil catalyzed by chlorosulfonic acid modified zirconia *via* simultaneous esterification and transesterification, *Bioresour. Technol.*, 2013, **147**, 59–64.

55 Y. Zhang, S. Niu, K. Han, Y. Li and C. Lu, Synthesis of the SrO–CaO–Al_2O_3 trimetallic oxide catalyst for transesterification to produce biodiesel, *Renew. Energy*, 2021, **168**, 981–990.

56 M. Anbia, S. Sedaghat, S. Saleh and S. Masoomi, Effect of synthesis method on the catalytic performance of Ca-Mg-Al mixed metal oxide nanocatalyst for biodiesel production from waste cooking oil, *Advanced Energy Conversion Materials*, 2021, **29**, 13–26.

57 B. Thangaraj, P. R. Solomon, B. Muniyandi, S. Ranganathan and L. Lin, Catalysis in biodiesel production—a review, *Clean Energy*, 2019, **3**(1), 2–3.

58 A. Guldhe, C. V. Moura, P. Singh, I. Rawat, E. M. Moura, Y. Sharma and F. Bux, Conversion of microalgal lipids to biodiesel using chromium-aluminum mixed oxide as a heterogeneous solid acid catalyst, *Renew. Energy*, 2017, **105**, 175–182.

59 O. Emmanuel, U. Micheal and M. Zafar, Elucidating the potential of non-edible milkweed seed oil for biodiesel production using green pod-derived nano-catalysts, *Waste Management Bulletin*, 2025, **3**(1), 27–38.

60 J. Gupta and M. Agarwal, Preparation and characterizaton of CaO nanoparticle for biodiesel production, in *AIP Conference Proceedings*, AIP Publishing, 2016, vol. 1724, no. 1.

61 B. H. Jume, M. A. Gabris, H. R. Nodeh, S. Rezania and J. Cho, Biodiesel production from waste cooking oil using a novel heterogeneous catalyst based on graphene oxide doped metal oxide nanoparticles, *Renew. Energy*, 2020, **162**, 2182–2189.

62 T. Lin, S. Zhao, S. Niu, Z. Lyu, K. Han and X. Hu, Halloysite nanotube functionalized with La-Ca bimetallic oxides as novel transesterification catalyst for biodiesel production

with molecular simulation, *Energy Convers. Manage.*, 2020, **220**, 113138.

63 S. Sahu, K. Saikia, B. Gurunathan, A. Dhakshinamoorthy and S. L. Rokhum, Green synthesis of CaO nanocatalyst using watermelon peels for biodiesel production, *Mol. Catal.*, 2023, **547**, 113342.

64 K. Krisnangkura, T. Yimsuwan and R. Pairintra, An empirical approach in predicting biodiesel viscosity at various temperatures, *Fuel*, 2006, **85**(1), 107–113.